TITLE

Rapid adaptive evolution of microbial thermal performance curves

SHORT TITLE

Evolution of microbial thermal performance curves

AUTHORS

Megan H. Liu[1*], Ze-Yi Han[1], Yaning Yuan[1], Katrina DeWitt[1], Daniel J. Wieczynski[1], Kathryn M. Yammine[2], Andrea Yammine[1], Rebecca Zufall[3], Adam Siepielski[4], Douglas Chalker[5], Masayuki Onishi[1], Fabio A. Machado[6], Jean P. Gibert[1*]

AFFILIATIONS

[1]Department of Biology, Duke University, Durham, NC, 27708, USA
[2]Department of Chemistry, Massachusetts Institute of Technology, Cambridge, MA, 02139, USA
[3]Department of Biology and Biochemistry, University of Houston, Houston, TX 77204, USA
[4]Department of Biological Sciences, University of Arkansas, Fayetteville, AR, USA
[5]Department of Biology, Washington University, Saint Louis, MI, USA
[6]Department of Integrative Biology, Oklahoma State University, Stillwater, OK, USA
*Corresponding author—email: mhliu58@gmail.com, jean.gibert@duke.edu

KEYWORDS:

Thermal Adaptation, Thermal Performance Curve Heritability, Climate Change, Quantitative Genetics

STATEMENT OF AUTHORSHIP:

All authors contributed to the conceptual foundation of the study. MHL, ZH, and JPG designed the study. DC contributed the fluorescent lines and provided cell biology expertise along with MO. MHL, ZH and AY collected the data. MHL and JPG performed data analyses with support from DHW, RZ, and AS. JPG did the mathematical modeling and FAM the quantitative genetics. MHL and JPG wrote the first draft of the manuscript and all authors contributed significantly to revisions.

DATA ACCESSABILITY STATEMENT

All software and data from this study are available on GitHub (https://github.com/JPGibert/TPC_evolution).

COUNTS

Abstract words: [148] | Main text words: [4867] | References: [72] | Figures: [4] | Tables: [0]

To whom correspondence should be addressed: mhliu58@gmail.com, jean.gibert@duke.edu

ABSTRACT

Microbial respiration is a key biotic driver of climate change. Warming boosts microbial population growth, which increases biomass and respiration. This feedback might be disrupted by adaptation in thermal performance curves (TPCs) –whose shape describes how temperature drives growth. In this study, we uncover substantial genetic variation (G) in microbial intrinsic population growth rates (*r*), demonstrate a causal link between G variation in *r* and G variation in TPC shape, and show how this variation constrains r-TPC shape evolution along specific evolutionary paths across temperatures. We also uncover Gene-by-Environment (G × E) variation in *r*, which results in specific signatures in TPC shape and predictable temperature-dependent rapid TPC evolution but also lower G, which could reduce future evolutionary potential. Overall, we show how temperature-dependent evolution in a linchpin of global ecosystem function—microbial TPC shape—is determined by a combination of heritable and non-heritable variation in intrinsic growth rates.

INTRODUCTION

Microbes play a central role in regulating the global carbon (C) cycle that controls climate change (Falkowski *et al.* 2008). Indeed, soil microbial respiration releases ~94Pg/yr of C into the atmosphere (Stell *et al.* 2021) while microalgae fix 30-50 Pg of C/yr globally (Falkowski 1994). Global warming is expected to alter these microbial processes (IPCC 2023), but anticipating these effects requires a deeper understanding of the biotic and abiotic factors influencing microbial respiration in a warming world (Rocca *et al.* 2022; Wieczynski *et al.* 2023).

One such factor is microbial population growth, which influences total standing biomass, and hence, total microbial respiration (Savage *et al.* 2004). The thermal performance curve of intrinsic population growth rate (*r*) describes how microbial population growth changes with temperature ('*r*-TPCs' henceforth, Fig 1). The shape of r-TPCs is controlled by temperature-dependent metabolism: metabolism increases with temperature, and so does *r*, until an 'optimal' temperature (T_{opt}) is reached (Fig 1a), then *r* declines as metabolic costs increase (Fig 1a; Amarasekare & Savage 2012). While *r*-TPC shape varies across species (Jacob & Legrand 2021;), unimodal shape is the norm (Wieczynski *et al.* 2021), described by shape parameters linked to thermal ecology: maximum growth rate (r_{peak}), minimum and maximum temperatures for population growth (CT_{min} and CT_{max} respectively), and rates of *r*-TPC increase/decrease with temperature (E_a, E_d respectively, Fig 1b). Ultimately, differences in *r*-TPC shape across species reflect divergent evolutionary trajectories in shape parameters across species and environments (Angilletta 2009).

While *r*-TPC shape is expected to evolve in novel environments, anticipating this thermal adaptation is a major open question, as the r-TPC reflects a species' ability to cope with

environmental change. Thermal adaptation hinges on the evolution of intraspecific—heritable—genetic variation and selection favoring genetic variants suited to novel environments (Frankham 2005), so quantifying heritable intraspecific variation in *r*-TPC shape parameters is central to understanding *r*-TPC shape evolution (Kling *et al.* 2023). From a quantitative genetics standpoint, the *r*-TPC represents the reaction norm of the underlying measure of performance, *r*, across temperatures among genotypes (Golmulkiewicz *et al.* 2018). *r*-TPC intraspecific variation is thus inextricably linked to that of *r*. Understanding this link is key to quantifying heritable variation in *r*-TPC shape parameters and predicting their response to selection in novel environments.

To understand the link between intraspecific variation in *r* and *r*-TPC shape parameters, we developed a verbal model using classic quantitative genetics of reaction norms (Fig 1, c-e). First, environmental variation (E) in *r*, driven by differential expression of *r* across temperatures, but not genotypes, classically manifests as completely overlapping genotypic reaction norms (Fig 1C, first row). Correspondingly, genotypic *r*-TPCs should also overlap (Fig 1D, first row) as they are reaction norms extended over multiple temperatures. Overlapping *r*-TPCs have no variation in shape parameters (Fig 1e, first row), so E in *r* should not result in *r*-TPC shape parameter variation. Second, genetic variation (G) in *r*, arising from differential expression of *r* across genotypes, but not temperatures, results in "additive" shifts in the intercepts of genotypic reaction norms—but equal slopes (Fig 1C, second row). These additive shifts translate to parallel *r*-TPCs (Fig 1D, second row), with additive variation in their x-axis intercepts (CT_{min}, CT_{max}) and their maximum height (r_{peak}), but no variation in T_{opt}, E_a, E_d (Fig 1E, second row). Last, gene-by-environment (G × E) interactions in *r*, which manifest as changes in intercept and slope of reaction norms across genotypes and temperatures (Fig 1C, third row), result in non-parallel *r*-

111 TPCs (Fig 1D, third row), with greater variation in all shape parameters (Fig 1E, third row). This
112 conceptual model therefore predicts covariation between heritable genetic variation in *r* and
113 variation in CT_{min}, CT_{max}, and r_{peak}, so *r*-TPCs' CT_{min}, CT_{max}, and r_{peak} are more likely to be
114 heritable and respond to selection than T_{opt} , E_a, or E_d, which in turn suggest constraints operating
115 on possible *r*-TPC evolutionary trajectories.

116 To address how *r*-TPC shape might evolve across temperatures we thus quantify E, G,
117 and G × E variation in *r*, and test predictions from our conceptual model. In doing so we reveal
118 that heritable variation in *r* results in substantial heritable variation in predicted shape
119 parameters. We build upon this understanding to quantify the structure of genetic variation and
120 covariation in shape parameters, and use this information to infer selection and possible *r*-TPC
121 evolutionary trajectories of shape parameters across temperatures. Last, we uncover a
122 mechanism of rapid *r*-TPC evolution in the presence of G × E variation in *r* that leads to
123 temperature-dependent selection on *r*-TPC shape, but can erase heritable variation, possibly
124 creating an evolutionary trap that constrains future microbial *r*-TPC evolution.

125

126 **METHODS**

127 *Study system and genotypes*

128 We used *Tetrahymena thermophila*, a freshwater ciliate protist found across the
129 Northeastern United States (Zufall *et al.* 2013) and part of a cosmopolitan genus (Lynn &
130 Doerder 2012). Protists, unicellular Eukaryotes that dominate oceanic biomass and rank third in
131 terrestrial biomass, comprise twice the biomass of the Animal Kingdom (Bar-On *et al.* 2018) and
132 underpin global ecosystem functioning (Gao *et al.* 2019). So, while no single species is

133 representative of the entire group, understanding thermal adaptation in such an ecologically
134 pivotal group is meaningful.
135 To do so, we sourced 22 unique *T. thermophila* genotypes: 19 from the Cornell
136 *Tetrahymena* Stock Center and 3 from the Chalker lab (Washington University, Appendix 1).
137 These genotypes, which vary in geographic origin and have well-known genetic differences
138 (Appendix 1), were chosen to sample existing genetic variation, not for their functional
139 significance. As most were derived from laboratory cultures, our assemblage likely contains less
140 variation than natural populations (Zufall *et al.* 2013), making our results a conservative estimate
141 of how thermal adaptation might proceed in nature.
142
143 *Quantifying r, r-TPCs, and TPC shape parameters*
144 Culture care and maintenance followed standard practices for ciliate Ecology (Appendix
145 2). Stock cultures were maintained in Percival AL-22 growth chambers with a 12hr day-night
146 cycle at 22°C. We quantified *r*-TPCs for all genotypes through growth assays in 3cm diameter
147 Petri dish microcosms containing 3mL of growth medium at seven temperatures (13, 19, 22, 25,
148 30, 32, 38°C). Each genotype and temperature combination was replicated six times, totaling 924
149 microcosms. Experimental temperatures span below and above the average growing season
150 temperature in *T. thermophila*'s native range (~23ºC ; NOAA 2024). Microcosms were
151 initialized at densities of 1ind/mL in 3ml Petri dishes, which results in exponential growth for 1-
152 2 days (Gibert *et al.* 2022, 2023; Singleton *et al.* 2021). After 24hrs, we censused the
153 microcosms through whole-population counts under a stereomicroscope (Leica M205C) and
154 calculated *r* across temperatures to characterize the entire *r*-TPC as log(final density/initial
155 density)/time, with time = 1 day (Wieczynski *et al.* 2021). To obtain *r*-TPC shape parameters, we

156 fitted a Sharpe-Schoolfield model ("nls.multstart" v1.3.0 package in R, (Padfield 2023)). Shape
157 parameters E_a, r_{peak}, CT_{min} and T_{opt} (Fig 1b) could be unequivocally estimated from our data, and
158 so we focused all subsequent analyses on those. These parameters control the rising portion of
159 the *r*-TPC (Fig 1b, green) –the "operational temperature range" (DeLong *et al.* 2017), i.e., what
160 most organisms are likely to experience in their native geographic ranges.
161
162 *Link between heritable genetic variation in r, and r-TPC shape parameters*
163 We quantified E, G and G × E variation in *r* using function *gxeVarComps*() in R package
164 statgenGxE v1.0.5. The function fits a linear model with *r* as the response variable, and
165 temperature, genotype, and their interaction as fixed predictors, to calculate effect sizes and
166 statistical significance. It then fits a second model with all fixed terms treated as random effects
167 to calculate *r* variance components (E, G, and G × E). Only G is considered to be heritable, so
168 the fraction of heritable genetic variation in *r*, can be estimated as the broad-sense heritability
169 (H^2=G/(E+G+G × E)). However, this expression does not account for inter-treatment and
170 replicate variability, which inflates E and underestimates H^2 (Cullis *et al.* 2006; Piepho &
171 Möhring 2007). In the appendix we present three alternative formulations for H^2 that address this
172 issue (Appendix 3).
173 Next, we tested the predictions of our verbal model (Fig 1) linking heritable variation in *r*
174 (G) to heritable variation in *r*-TPC shape parameters. Since each *r*-TPC yields a single shape
175 parameter set, only G variation in shape parameters could be quantified. All other components of
176 variation (e.g., E, G × E, error) were pooled as residual variance. To evaluate the model's
177 prediction that G variation in *r* results in greater G variation in shape parameters r_{peak} and CT_{min}
178 compared to E_a, and T_{opt} (Fig 1e), we tested whether r_{peak} and CT_{min} exhibited stronger genetic

179 covariance with *r* than did E_a, and T_{opt} using a multivariate Bayesian Generalized Linear Mixed
180 Model. The model includes mean-scaled values of *r*, E_a, r_{peak}, CT_{min} and T_{opt} as jointly modeled
181 response variables, each with their own fixed mean, and Genotype as a random effect to estimate
182 variances and covariances implemented in R package MCMCglmm v.2.36 (Hadfield 2010).
183 Variance-covariance priors were obtained by bootstrapping *r*-TPC data 100 times within each
184 genotype and re-fitting the Sharpe-Schoolfield model to each bootstrap replicate, generating a
185 population of shape parameters for each genotype (Appendix 4). Using inverse Wishart priors
186 (Murphy 2012) did not alter our results. Last, if G variation in *r* results in greater G in r_{peak} and
187 CT_{min}, these shape parameters should also have greater heritability than E_a, and T_{opt}. To confirm
188 this, we calculated the broad-sense heritability in *r*-TPC parameters using the standard
189 expression H^2=G/(G+residual variance) with G and residual variance estimates from the
190 MCMCglmm model.
191
192 *Consequences of heritable variation: selection and evolutionary potential of r-TPC parameters*
193 Heritable *r*-TPC shape parameters can evolve under selection. To understand how, we
194 quantified 1) the direction, form, and magnitude of selection on all four shape parameters, 2)
195 whether and how temperature influenced selection, and, 3) their potential evolutionary responses
196 across temperatures. We used two approaches: one that neglects genetic correlations between
197 parameters but allows estimation of non-linear selection (e.g., stabilizing selection), and one that
198 accounts for genetic correlations and neglects non-linear selection, while enabling predictions of
199 evolutionary responses across temperatures.
200 In the first approach, we quantified selection by characterizing the adaptive landscape
201 (Lande 1976, 1979) as the relationship between shape parameter values and absolute fitness—

classically assumed to a function of *r* (Lande 1976, 1979) because it reflects average birth and death rates of individuals, two major fitness components (Lande 1982; Partridge & Harvey 1988). We modeled this relationship for all shape parameter values fitted across genotypes, using polynomial regression and *r* as the response, linear and quadratic effects (i.e., non-linear selection) for each mean-standardized shape parameter, and additive and interactive temperature effects with the linear and quadratic shape parameter terms (see Appendix 5). We multiplied the quadratic regression coefficient by two (Stinchcombe *et al.* 2008). A positive relationship between *r* and the focal shape parameter would be evidence of positive directional selection, a negative relationship would indicate negative directional selection, and no relationship suggests no directional selection. Stabilizing selection would result in a concave-down relationship, and disruptive selection would manifest as a concave-up relationship where extreme values have higher fitness (Lande & Arnold 1983).

The second approach predicts *r*-TPC shape evolution across temperatures while accounting for genetic correlations among shape parameters. It uses the multivariate breeder's (Lande 1979) and Price's (Price 1972) equations to estimate direct (i.e., acting on the focal parameter) and indirect selection (i.e., acting on genetically linked parameters, (Stinchcombe *et al.* 2014)). This is achieved by estimating the response to selection of all shape parameters, $\mathbf{\Delta z}$, as their covariance with fitness—i.e., the Price equation aspect of this approach– which requires estimating a genetic variance-covariance matrix ($\mathbf{G_{zw}}$)—i.e., its multi-variate breeder's equation aspect. This matrix includes the genetic variance-covariance matrix (**G**) of shape parameters as its first four rows/columns, and their genetic covariation with fitness (W) as the last row/column (Lande 1976, 1979, 1982). The finite rate of increase R=*exp(r)* was used as our metric of fitness but using plain *r* did not alter our results. From the Price equation, this last row/column also

225 equals the vector of predicted trait change, $\mathbf{\Delta z}$, so $\mathbf{G_{zw}}$ also yields $\mathbf{\Delta z}$. Then, from the multivariate
226 Breeder's equation, $\mathbf{\Delta z} = \mathbf{G\beta}$, where $\boldsymbol{\beta}$ is the selection gradient (Lande 1979). Provided that **G** is
227 invertible, then $\boldsymbol{\beta} = \mathbf{G}^{-1}\,\mathbf{\Delta z}$, to estimate selection.

228 Positive/negative Δz_i values indicate an increase/decrease in the i-th shape parameter,
229 while positive/negative β_i, indicates positive/negative selection operating on the i-th shape
230 parameter. Alignment between Δz_i and β_i indicates direct responses to selection (Hansen &
231 Houle 2008), in our case, by temperature, while misalignment suggest indirect selection through
232 correlated responses with other shape parameters.

233 To estimate $\mathbf{G_{zw}}$ for each temperature, we used subsets of *r* for each genotype for each
234 temperature. Shape parameters do not change across temperatures but *r* does, so the $\mathbf{G_{zw}}$ matrices
235 only differed in their last row/column across temperatures, i.e., the covariances between shape
236 parameters and fitness—or $\mathbf{\Delta z}$. To facilitate this estimation and ensure interpretability, all $\mathbf{G_{zw}}$
237 variables were rescaled, which was achieved through the expression $\mathbf{G_{zw}}$ as $=\mathbf{SLS}^*(1/2F)$ where
238 **L** is a between-genotype covariance matrix, **S** is a diagonal matrix containing the inverse of each
239 trait's standard deviation, and F is the inbreeding coefficient, which equals 1 for clonal lineages
240 (Falconer 1996). We quantified uncertainty in $\mathbf{G_{zw}}$ entries using a Bayesian posterior distribution
241 of **L** matrices (and hence $\mathbf{G_{zw}}$) and used a multivariate normal likelihood function and non-
242 informative inverse regularized Wishart priors (nu=traits+1) (Murphy 2012), implemented in
243 evolqg v3.0 R package (Melo *et al.* 2015). Using MCMCglmm instead of evolqg did not affect
244 our results (Appendix 6). We took 1000 posterior samples for $\mathbf{G_{zw}}$ to calculate $\mathbf{\Delta z}$, **G**, and $\boldsymbol{\beta}$, and
245 95% maximum density intervals for al estimates.

246

247 *Consequences of G × E in r for rapid r-TPC evolution*

248 Because G × E variation in *r* is predicted to result in non-parallel *r*-TPCs (Fig 1), slight
249 differences in intrinsic growth rates across temperatures can drive temperature-mediated
250 differential selection among genotypes (Fig 4a, b). Treating *r* as proxy for absolute fitness
251 (Lande 1976), this selection should be strongest at temperatures where *r*-TPCs differ the most,
252 i.e., the temperatures with the largest differences in relative fitness.

253 We empirically tested for temperature-dependent selection among genotypes by setting
254 up an experimental evolution assay with two fluorescently marked strains (AXS and CU4106,
255 Fig 4c) with different *r*-TPCs and relative fitness (Fig 4d, Fig4d inset) across six temperatures
256 (19, 22, 25, 30, 32, 38ºC), each replicated seven times, and 2 additional single-strain controls per
257 temperature. The genotypes cannot mate because they belong to the same mating type (mating
258 type VII, Appendix 1), so only clonal reproduction was possible. We initialized our microcosms
259 at equal densities (5 ind/mL in mixture treatments, 10ind/mL for single-genotype controls). After
260 48 hours, we added Cadmium Chloride to induce fluorescence (Appendix 7), confirmed on a
261 Leica Thunder Cell Culture inverted microscope (Fig 4c and Appendix 8). Thirty minutes later,
262 we cytometrically censused each sample (Novocyte 2000R). While fluorescently tagged
263 genotypes can lose their ability to fluoresce over time, they carry a paromomycin resistance gene
264 (Appendix 7), allowing selection through paromomycin exposure (100µg/mL) prior to counting
265 and estimating relative frequencies based on fluorescence (Appendices 9-10). Antibiotics can
266 negatively affect protists and the bacterial communities they feed on, so we replicated this
267 experiment in paromomycin-free conditions, which did not qualitatively alter our results (see
268 Appendix Fig S11).

269 Last, observed changes in genetic frequencies were compared to predicted frequencies by
270 a classic model of genetic evolution in discrete time parameterized with the *r*-TPC of both

experimental genotypes (Fig 4f). The model tracks the frequency of each strain f_i, and assumes that their absolute fitness, W_i, is a function of their average intrinsic growth rate *r* (Lande 1976, 1979). The frequency of each strain in the population is determined by the classic recursive equation, $f_i(t+1) = f_i(t)(W_i/\overline{W})$ [Eq 1.], where $\overline{W}$ is the average fitness of the population ($\sum_{i=1}^{n} f_i W_i = \sum_{i=1}^{n} f_i r_i$), and $W_i/\overline{W}$ is fitness the relative fitness of i-th genotype *relative* to the entire population. We used each genotype's *r*-TPC (AXS, CU4106, Fig 4d) to estimate $W_i/\overline{W}$ across temperatures (i.e., replacing r_i). We forward-solved the recursive equation (Eq 1) under two scenarios: one in which temperature was constant, and one in which temperature fluctuated randomly across generations, drawn from a normal distribution with known mean and variance. This minimal model assumes that differential selection across environments is mostly driven by differences in *r*-TPCs, and disregards density- and frequency-dependent selection, sexual reproduction, mutation, and most all ecological processes.

RESULTS

Heritable variation in r leads to heritable variation in r-TPC shape parameters

Intrinsic growth rates showed strong temperature responses within genotypes ($F = 3092.70$, $D_f = 6$, Generalized Eta-Squared (GES) effect size = 0.964, $p \leq 0.001$), significant variability across genotypes ($F = 163.65$, $p \leq 0.001$, $D_f = 21$, GES = 0.832), and significant G × E interactions ($F=29.7$, $p \leq 0.001$, $D_f = 122$, GES = 0.840), leading to classically unimodal shapes that varied among genotypes (Fig 2a). Environmental variation (E) accounted for 71.7% of all observed variation in *r*, genetic variation (G) explained 6.1% of all variation, and Gene-by-Environment interactions (G × E) explained 11.7%, with 10.5% residual variation (Fig 2b). This is well within what is expected for life history traits (Hoffmann & Sgrò 2011). Despite a

294 relatively modest G compared to E, after accounting for experimental inter-treatment and
295 replicate variability, *r* was strongly heritable ($H^2_{standard}$=0.76, H^2_{cullis}=0.95, H^2_{piepho}=0.91,
296 Appendix 3).

297 Shape parameters varied widely across genotypes (e.g., genotype AXS was 3.2 times
298 more thermally sensitive than A1868 and could grow 3.6 times faster at T_{opt}, Fig 2, and
299 Appendices 12-13). As predicted, CT_{min} and r_{peak} showed strong genetic covariation with *r* (|
300 $Gcov_{CTmin}$ | = 0.65, | $Gcov_{rpeak}$ | = 0.63, Appendix 14), but there was no evidence of genetic
301 covariation between *r* and T_{opt} or E_a (credible intervals contained 0, Appendix 14). Last, shape
302 parameter heritabilities matched verbal model predictions (H^2_{CTmin}=0.945, H^2_{rpeak}=0.949,
303 H^2_{Topt}=0.070, H^2_{Ea}=0.002), confirming that heritable variation in *r* results in heritable variation in
304 CT_{min} and r_{peak}, but not T_{opt} or E_a.

305

306 *Consequences of G in r: selection and evolvability of r-TPC shape parameters*

307 Without accounting for genetic covariances, selection operated differentially across shape
308 parameters and was temperature dependent: r_{peak} was under negative directional selection at low
309 temperatures (<20°C, Fig 3a, Appendix 15), weakly positive or no directional selection at
310 intermediate temperatures (between 20 and 30°C, Fig 3a, Appendix 15), and strong positive
311 directional selection in high temperatures with E_a following a similar pattern (Fig 3b, Appendix
312 16). CT_{min} was under negative selection at low/intermediate temperatures but no selection at high
313 temperatures (Fig 3c, Appendix 17). Last, T_{opt} was under no selection at low temperatures but
314 under weak then strong stabilizing selection at intermediate and high temperatures, respectively
315 (Fig 3d, and Appendices 18-19).

316 However, we also found clear positive genetic covariances between r_{peak} and E_a, CT_{min}
317 and E_a, and CT_{min} and T_{opt} (Fig 3e). Consequently, selection acting on highly heritable
318 parameters CT_{min} and r_{peak} could still result in correlated evolution in weakly heritable parameters
319 E_a, and T_{opt}. Accounting for these genetic covariances, we confirmed differences in selection
320 across shape parameters whose magnitude and direction also shifted with temperature (Fig 3f),
321 resulting in possible temperature-dependent shifts in parameters (Fig 3g). Specifically, our
322 multivariate analysis suggested that selection would favor higher r_{peak} (and maybe E_a) at high
323 temperatures, and low E_a and CT_{min} at low temperatures, but no selection on T_{opt} (Fig 3f),
324 generally matching univariate predictions (Fig 3g). Overall, the evolutionary responses followed
325 predicted trajectories from the estimates of selection closely (Fig 3f-g), with a few exceptions
326 that suggest correlated evolution: positive response of E_a with temperature likely are correlated
327 responses with r_{peak} (Fig 3g), which in turn shows strong negative response at low temperatures
328 despite no selection, likely through correlated evolution with E_a whose negative response is
329 driven by negative selection in CT_{min} (Fig 3g). Despite differences in heritability which impose
330 constraints in r-TPC evolution, genetic correlations among shape parameters allowed for
331 temperature-dependent evolutionary responses in all of them except T_{opt}, which our results
332 suggest is under stabilizing selection (Fig 3d).
333
334 *Consequences of G × E in r: sorting of standing genetic variation across temperatures*
335 We observed significant temperature-dependent differential selection among genotypes
336 (Fig 4e), matching theoretical predictions from a simple model of genetic evolution (Fig 4f),
337 which confirms the hypothesis that G × E in *r* could set the stage for rapid r-TPC shape evolution
338 through selection on standing genetic variation (Fig 4a, b). Despite quantitative discrepancies

339 between observed and predicted frequencies—notably at 19ºC where the model predicted a
340 polymorphic population but the data indicated otherwise (Fig 4e, f)—it still correctly predicted
341 observed changes in genetic frequencies across most temperatures. These results are also robust
342 to different experimental conditions (Appendix 11) and fluctuating temperatures (Appendix 20),
343 the latter showing that temperature fluctuations could play a role in determining r-TPC evolution
344 if *r*-TPCs show multiple crossing points in a short temperature span.

345 The results of this experiment were also consistent with our estimated predicted
346 responses to selection (cf. Fig 3 and Fig 4): lower temperatures led to higher frequencies of the
347 CU4106 genotype, whose *r*-TPC has lower E_a and CT_{min} compared to AXS (Fig 4d), so the
348 average *r*-TPC of the population should reflect that and also have lower E_a and CT_{min}, as
349 predicted by our multivariate model. At higher temperatures, selection favored AXS, which has
350 higher E_a, so the ensuing population also should have an average *r*-TPC with higher E_a (Fig 4d).
351 Last, rising temperatures led to an increase in genetic variance (~p(1-p) where p is the frequency
352 of either genotype and 1-p that of the other) compared to lower temperatures (Fig 4e, f)—which
353 should facilitate adaptation—then a reduction in genetic variance (as genotype CU4106 becomes
354 less prevalent, Fig 4e, f), which in turn could impede adaptive evolution in the future.

355

356 **DISCUSSION**

357 Our study reveals heritable genetic variation in *Tetrahymena thermophila*'s population
358 intrinsic growth rates that results in heritable variation in some, but not all, *r*-TPC shape
359 parameters (Fig 2), allowing for thermal adaptation in new climates (Fig 3). Observed *intra*-
360 specific variation in *r*-TPC shape parameters rivals reported *inter*-specific variation across
361 multiple protist species (Wieczynski *et al.* 2021). We also found that most *r*-TPC shape

362 parameters are under different selection regimes across temperatures (Fig 3), with parameters
363 CT_{min} and r_{peak} being more likely to respond to selection than E_a and T_{opt}, but even weakly-
364 heritable parameters can still evolve through correlated evolution (Fig 3). Consequently, colder
365 temperatures select for lower CT_{min}, r_{peak}, and E_a, and warmer temperatures lead to high r_{peak} and
366 E_a (Fig 3). Last, we showed that G × E in *r* can lead to rapid, predictable shifts in population
367 genetic makeup across temperatures and *r*-TPC evolution (Fig 4), in a "plasticity drives
368 adaptation" scenario (Ghalambor *et al.* 2007).

369 While the evolution of microbial TPCs is likely the product of adaptation to local habitats
370 (Kontopoulos *et al.* 2020), how *r*-TPCs will adapt to ongoing rising temperatures remains an
371 open question. Several canonical evolutionary paths have been proposed: 1)'Colder-is-Better'
372 (CIB), where rising temperatures reduce population growth, leading to lower r_{peak}, T_{opt}, and E_a
373 (Kingsolver & Huey 2008). 2) Warmer-Is-Better (WIB), where higher growth rates evolve in
374 warmer temperatures, leading to TPCs with higher r_{peak} and T_{opt} (Pawar *et al.* 2015). And, 3)
375 Generalist-Specialist-Tradeoff (GST), where species can either evolve towards rapid growth
376 within a narrow temperature range (i.e., temperature specialists), or slower growth over a broader
377 temperature range (i.e., temperature generalists), leading to higher r_{peak}, higher CT_{min}, and lower
378 CT_{max} (Seebacher *et al.* 2015). Tests of these possible evolutionary paths (Kontopoulos *et al.*
379 2020; Montagnes *et al.* 2022) mostly use inter-species comparisons that often overlook intra-
380 specific variation and genetic associations between shape parameters, and therefore cannot
381 readily make predictions about *r*-TPC evolutionary trajectories for any given species. Indeed,
382 without accounting for genetic associations, our results would suggest support for WIB with
383 clear directional selection for higher r_{peak} and E_a under warming climates (Fig 3a, b). Accounting
384 for genetic covariances, however, suggested more complex evolutionary *r*-TPC responses than

385 currently predicted by theory. Specifically: we show support for WIB as warming should favor *r*-
386 TPCs with high r_{peak} and high E_a (Fig 3f, g), but no support for GST, as CT_{min} and r_{peak} responded
387 mostly together (Fig 3f, g). Last, T_{opt} is assumed to evolve under WIB, CIB and GST, but we
388 found no selection (Fig 3f) –or maybe even weakly stabilizing selection (Fig 3d)– and no
389 evolutionary response (Fig 3g). This suggesting that neither WIB, CIB and GST can explain
390 predicted evolutionary responses in *T. thermophila*, which emphasize the importance of
391 intraspecific variation and genetic associations to fully understand *r*-TPC evolution.

392 When G × E in *r* is prevalent, we showed that thermal adaptation can occur rapidly
393 through temperature-dependent selection on *r*-TPC genotypes (Fig 4), resulting in reduced
394 genetic variation. Loss of G which could slow down, or impede, future adaptation (Pauls *et al.*
395 2013). In other words, we show that phenotypic plasticity in *r* could lead to adaptive evolution in
396 r-TPCs in novel climates. That this form of r-TPC evolution could be anticipated from simple
397 models of genetic evolution, is striking, considering how little information beyond the r-TPC of
398 each genotype the model accounts for. Yet, *r*-TPC adaptation in deep time has been suggested to
399 occur gradually across six different *Tetrahymena* species (Montagnes *et al.* 2022), directly
400 countering our claim that *r*-TPCs could evolve rapidly through temperature-dependent selection.
401 We argue that this form of rapid *r*-TPC evolution may only play out during fast-changing
402 environmental conditions, not always result in long-term *r*-TPC change, or be masked by
403 reversals in selection. In fact, selection often "erases its traces" (Haller & Hendry 2014), and is
404 strongest under novel conditions, weakening as populations adapt (Caruso *et al.* 2017)—i.e., "the
405 paradox of stasis" (Haller & Hendry 2014).

406 Resulting temperature-dependent loss of genetic diversity of adaptive r-TPC evolution
407 could impact the persistence of genetically depauperate species under warming. But whether this

408 may be the case in nature hinges on quantifying processes that generate diversity (mutation, gene
409 flow, recombination) in *r* and *r*-TPC shape parameters in the wild, and assessing when these
410 processes could counter loss of genetic diversity after episodes of thermally-induced *r*-TPC
411 evolution. *T. thermophila* has the lowest reported base substitution mutation rate of all species
412 (Zufall et al. 2016), and limited gene flow (Zufall et al. 2013), but even weak dispersal or rare
413 mutation events could contribute to *r* and *r*-TPC variation and rescue genetic diversity in very
414 large, rapidly reproducing populations. The prevalence of sexual reproduction in nature is
415 debated –e.g. ~50% of wild individual *T. thermophila* cannot reproduce sexually and some
416 *Tetrahymena* lineages have lost this ability entirety (Doerder 2014)– but likely important if
417 present. In fact, *T. thermophila* possesses two separate genomes, a germinal line (in
418 micronucleus) and an expressed genome (in macronucleus). Our study focuses on macronuclear
419 variation, but asexual reproduction following sex results in random distribution of macronuclear
420 alleles to daughter cells—i.e. phenotypic assortment—potentially generating novel variation in r
421 and r-TPCs (Tarkington *et al.* 2023). Moreover, seemingly lost genetic variation could persist in
422 the population in other individual's micronuclei and reemerge following sexual reproduction
423 (Dimond & Zufall 2016). Fully understanding thermal adaptation in nature thus requires
424 exploring these processes' interplay, yet, for most organisms, they remain poorly understood.
425
426 *Caveats*
427 While bodies of water in *T. thermophila*'s native range are warming significantly (US EPA
428 2021) and experiencing more frequent and extreme heatwaves (Tassone *et al.* 2023), water
429 temperature typically remains 2-5ºC cooler than air temperature (Stefan & Preud'homme 1993).
430 Thus, some of the warmer temperatures in our study may be uncommon in *T. thermophila*'s

native range. However, strong temperature effects observed at low temperatures suggest these patterns can still operate in many *T. thermophila* populations. Also, previous research showed that most variation in *r*-TPC shape across species could be collapsed into a single dimension of variation (Rezende & Bozinovic 2019), suggesting that some of the covariation observed in this study between shape parameters could be spurious. If these *r*-TPCs could actually be collapsed into a single axis of variation, however, we would have expected strong and multiple covariation between most if not all shape parameters—which was not the case (Fig 3e, f). Interestingly, most of the genetic variation in shape parameters was observed, as predicted, in CT_{min} and r_{peak}, but these two parameters were not correlated to one another. Perhaps our intraspecific *r*-TPC variation results stand in contrast to those observed across species (Rezende and Bozinovic, 2019), but more research is needed to clarify this point.

Conclusion

Overall, TPCs control the fate of populations (Sinclair *et al.* 2016), ecological interactions (Enquist *et al.* 2015), food web dynamics (Barbour & Gibert 2021; Gibert *et al.* 2022), and ecosystem processes (Gibert *et al.* 2015). Yet, TPC evolution in a rapidly warming world remains conspicuously unknown. Here, we show that *r* intraspecific variation can drive temperature-dependent evolution in microbial *r*-TPCs and have consequences for rapid shifts in population genetic makeup. Despite studying a single protist species, our findings provide a foundation for studying thermal adaptation in this diverse and important microbial group and beyond. Our study emphasizes the importance of temperature in mediating rapid microbial evolutionary change as we grapple with understanding and predicting organismal responses to an increasingly warmer world.

ACKNOWLEDGMENTS

We are grateful to Enzo Bruscato and Heather Raslan for their data collection support. We are indebted to Samraat Pawar, John Stinchcombe, and two anonymous reviewers for their feedback on earlier versions of our manuscript. AMS was supported by NSF DEB award 2306183. DLC acknowledges grant support for the Tetrahymena Stock Center by NIH project # 2P40OD010964 and additional support from NSF award # MCB 1947526. JPG acknowledges generous support from DOE BER DE-SC0020362 (which also supported MHL, AY, and DJW), NSF DEB award number 2224819, NSF CAREER award number 2337107, and a Simons Foundation Early Career Fellowship in Microbial Ecology and Evolution LS-ECIAMEE-00001588 (which also supported MHL and AY).

REFERENCES

Amarasekare, P. & Savage, V. (2012). A Framework for Elucidating the Temperature Dependence of Fitness. *Am. Nat.*, 179, 178–191.

Angilletta, M.J. (2009). *Thermal Adaptation: A Theoretical and Empirical Synthesis*. OUP Oxford.

Antiqueira, P.A.P., Petchey, O.L. & Romero, G.Q. (2018). Warming and top predator loss drive ecosystem multifunctionality. *Ecol. Lett.*, 21, 72–82.

Arrigo, K.R. (2005). Marine microorganisms and global nutrient cycles. *Nature*, 437, 349–355.

Barbour, M.A. & Gibert, J.P. (2021). Genetic and plastic rewiring of food webs under climate change. *J. Anim. Ecol.*, 90, 1814–1830.

Bar-On, Y.M., Phillips, R. & Milo, R. (2018). The biomass distribution on Earth. *Proc. Natl. Acad. Sci.*, 115, 6506–6511.

Bideault, A., Loreau, M. & Gravel, D. (2019). Temperature Modifies Consumer-Resource Interaction Strength Through Its Effects on Biological Rates and Body Mass. *Front. Ecol. Evol.*, 7.

Bond-Lamberty, B. (2018). New Techniques and Data for Understanding the Global Soil Respiration Flux. *Earths Future*, 6, 1176–1180.

Caruso, C.M., Martin, R.A., Sletvold, N., Morrissey, M.B., Wade, M.J., Augustine, K.E., *et al.* (2017). What Are the Environmental Determinants of Phenotypic Selection? A Meta-analysis of Experimental Studies. *Am. Nat.*, 190, 363–376.

Cullis, B.R., Smith, A.B. & Coombes, N.E. (2006). On the design of early generation variety trials with correlated data. *J. Agric. Biol. Environ. Stat.*, 11, 381–393.

Davidson, E.A. & Janssens, I.A. (2006). Temperature sensitivity of soil carbon decomposition and feedbacks to climate change. *Nature*, 440, 165–173.

DeLong, J.P., Gibert, J.P., Luhring, T.M., Bachman, G., Reed, B., Neyer, A., *et al.* (2017). The combined effects of reactant kinetics and enzyme stability explain the temperature dependence of metabolic rates. *Ecol. Evol.*, 7, 3940–3950.

Dimond K.L., Zufall R.A (2016). Hidden genetic variation in the germline genome of Tetrahymena thermophila. J Evol Biol 29(6):1284-92

Doerder, F.P. (2014). Abandoning sex: multiple origins of asexuality in the ciliate Tetrahymena. *BMC Evol. Biol.*, 14, 112.

Enquist, B.J., Norberg, J., Bonser, S.P., Violle, C., Webb, C.T., Henderson, A., *et al.* (2015). Chapter Nine - Scaling from Traits to Ecosystems: Developing a General Trait Driver Theory via Integrating Trait-Based and Metabolic Scaling Theories. In: *Advances in Ecological Research*, Trait-Based Ecology - From Structure to Function (eds. Pawar, S., Woodward, G. & Dell, A.I.). Academic Press, pp. 249–318.

Falconer, D.S. (1996). *Introduction To Quantitative Genetics 4th Edition*.

Falkowski, P.G. (1994). The role of phytoplankton photosynthesis in global biogeochemical cycles. *Photosynth. Res.*, 39, 235–258.

Falkowski, P.G., Fenchel, T. & Delong, E.F. (2008). The Microbial Engines That Drive Earth's Biogeochemical Cycles. *Science*, 320, 1034–1039.

Frankham, R. (2005). Stress and adaptation in conservation genetics. *J. Evol. Biol.*, 18, 750–755.

Frazier, M.R., Huey, R.B. & Berrigan, D. (2006). Thermodynamics Constrains the Evolution of Insect Population Growth Rates: "Warmer Is Better." *Am. Nat.*, 168, 512–520.

Gao, Z., Karlsson, I., Geisen, S., Kowalchuk, G. & Jousset, A. (2019). Protists: Puppet Masters of the Rhizosphere Microbiome. *Trends Plant Sci.*, 24, 165–176.

Ghalambor, C.K., McKAY, J.K., Carroll, S.P. & Reznick, D.N. (2007). Adaptive versus non-adaptive phenotypic plasticity and the potential for contemporary adaptation in new environments. *Funct. Ecol.*, 21, 394–407.

Gibert, J.P., Dell, A.I., DeLong, J.P. & Pawar, S. (2015). Chapter One - Scaling-up Trait Variation from Individuals to Ecosystems. In: *Advances in Ecological Research*, Trait-Based Ecology - From Structure to Function (eds. Pawar, S., Woodward, G. & Dell, A.I.). Academic Press, pp. 1–17.

Gibert, J.P., Grady, J.M. & Dell, A.I. (2022). Food web consequences of thermal asymmetries. *Funct. Ecol.*, 36, 1887–1899.

Gibert, J.P., Wieczynski, D.J., Han, Z.-Y. & Yammine, A. (2023). Rapid eco-phenotypic feedback and the temperature response of biomass dynamics. *Ecol. Evol.*, 13, e9685.

Gillooly, J.F., Brown, J.H., West, G.B., Savage, V.M. & Charnov, E.L. (2001). Effects of size and temperature on metabolic rate. *Science*, 293, 2248–2251.

Golmulkiewicz, R., Kingsolver, J.G., Carter, P.A. & Heckman, N. (2018). Variation and Evolution of Function-Valued Traits. *Annu. Rev. Ecol. Evol. Syst.*, 49, 139–64.

Hadfield, J.D. (2010). MCMC Methods for Multi-Response Generalized Linear Mixed Models: The MCMCglmm R Package. *J. Stat. Softw.*, 33, 1–22.

Haller, B.C. & Hendry, A.P. (2014). Solving the paradox of stasis: squashed stabilizing selection and the limits of detection. *Evol. Int. J. Org. Evol.*, 68, 483–500.

Hansen, T.F. & Houle, D. (2008). Measuring and comparing evolvability and constraint in multivariate characters. *J. Evol. Biol.*, 21, 1201–1219.

Hoffmann, A.A. & Sgrò, C.M. (2011). Climate change and evolutionary adaptation. *Nature*, 470, 479–485.

IPCC. (2023). *Climate Change 2021 – The Physical Science Basis: Working Group I Contribution to the Sixth Assessment Report of the Intergovernmental Panel on Climate Change*. Cambridge University Press, Cambridge.

Jacob, S. & Legrand, D. (2021). Phenotypic plasticity can reverse the relative extent of intra- and interspecific variability across a thermal gradient. *Proc. R. Soc. B Biol. Sci.*, 288, 20210428.

Kingsolver, J. & Huey, R. (2008). Size, temperature, and fitness: Three rules. *Evol. Ecol. Res.*, 10, 251–268.

Kling, J.D., Lee, M.D., Walworth, N.G., Webb, E.A., Coelho, J.T., Wilburn, P., *et al.* (2023). Dual thermal ecotypes coexist within a nearly genetically identical population of the unicellular marine cyanobacterium Synechococcus. *Proc. Natl. Acad. Sci.*, 120, e2315701120.

Kontopoulos, D.-G., Smith, T.P., Barraclough, T.G. & Pawar, S. (2020). Adaptive evolution shapes the present-day distribution of the thermal sensitivity of population growth rate. *PLOS Biol.*, 18, e3000894.

Lande, R. (1976). Natural Selection and Random Genetic Drift in Phenotypic Evolution. *Evolution*, 30, 314–334.

Lande, R. (1979). Quantitative Genetic Analysis of Multivariate Evolution, Applied to Brain:body Size Allometry. *Evolution*, 33, 402–416.

Lande, R. (1982). A Quantitative Genetic Theory of Life History Evolution. *Ecology*, 63, 607–615.

Lande, R. & Arnold, S.J. (1983). The measurement of selection on correlated characters. *Evolution*, 37, 1210–1226.

Lynn, D.H. & Doerder, F.P. (2012). The life and times of Tetrahymena. *Methods Cell Biol.*, 109, 9–27.

MacColl, A.D.C. (2011). The ecological causes of evolution. *Trends Ecol. Evol.*, 26, 514–522.

Malusare, S.P., Zilio, G. & Fronhofer, E.A. (2023). Evolution of thermal performance curves: A meta-analysis of selection experiments. *J. Evol. Biol.*, 36, 15–28.

Melo, D., Garcia, G., Hubbe, A., Assis, A.P. & Marroig, G. (2015). EvolQG - An R package for evolutionary quantitative genetics. *F1000Research*, 4, 925.

Montagnes, D.J.S., Wang, Q., Lyu, Z. & Shao, C. (2022). Evaluating thermal performance of closely related taxa: Support for hotter is not better, but for unexpected reasons. *Ecol. Monogr.*, 92, e1517.

Murphy, K. (2012). *Machine learning: a probabilistic perspective*. MIT Press, Cambridge, MA.

NOAA. (2024). *NOAA NCEI U.S. Climate Normals Quick Access*. Available at: https://www.ncei.noaa.gov/access/us-climate-normals/#dataset=normals-monthly&timeframe=30&location=MA&station=USW00014739. Last accessed 23 January 2024.

Padfield, D. (2023). Robust Non-Linear Regression using AIC Scores.

Partridge, L. & Harvey, P.H. (1988). The Ecological Context of Life History Evolution. *Science*, 241, 1449–1455.

Pauls, S.U., Nowak, C., Bálint, M. & Pfenninger, M. (2013). The impact of global climate change on genetic diversity within populations and species. *Mol. Ecol.*, 22, 925–946.

Pawar, S., Dell, A.I. & Savage, V.M. (2015). Chapter 1 - From Metabolic Constraints on Individuals to the Dynamics of Ecosystems. In: *Aquatic Functional Biodiversity* (eds. Belgrano, A., Woodward, G. & Jacob, U.). Academic Press, San Diego, pp. 3–36.

Phillips, B.L., Llewelyn, J., Hatcher, A., Macdonald, S. & Moritz, C. (2014). Do evolutionary constraints on thermal performance manifest at different organizational scales? *J. Evol. Biol.*, 27, 2687–2694.

Piepho, H.-P. & Möhring, J. (2007). Computing Heritability and Selection Response From Unbalanced Plant Breeding Trials. *Genetics*, 177, 1881–1888.

Price, G.R. (1972). Extension of covariance selection mathematics. *Ann. Hum. Genet.*, 35, 485–490.

Rezende, E.L. & Bozinovic, F. (2019). Thermal performance across levels of biological organization. *Philos. Trans. R. Soc. Lond. B. Biol. Sci.*, 374, 20180549.

Rocca, J.D., Yammine, A., Simonin, M. & Gibert, J.P. (2022). Protist Predation Influences the Temperature Response of Bacterial Communities. *Front. Microbiol.*, 13.

Savage, V.M., Gillooly, J.F., Brown, J.H., West, G.B. & Charnov, E.L. (2004). Effects of Body Size and Temperature on Population Growth. *Am. Nat.*, 163, 429–441.

Seebacher, F., Ducret, V., Little, A.G. & Adriaenssens, B. (2015). Generalist–specialist trade-off during thermal acclimation. *R. Soc. Open Sci.*, 2, 140251.

Seebacher, F. & Little, A.G. (2021). Plasticity of Performance Curves in Ectotherms: Individual Variation Modulates Population Responses to Environmental Change. *Front. Physiol.*, 12.

Sinclair, B.J., Marshall, K.E., Sewell, M.A., Levesque, D.L., Willett, C.S., Slotsbo, S., *et al.* (2016). Can we predict ectotherm responses to climate change using thermal performance curves and body temperatures? *Ecol. Lett.*, 19, 1372–1385.

Singleton, A.L., Liu, M.H., Votzke, S., Yammine, A. & Gibert, J.P. (2021). Increasing temperature weakens the positive effect of genetic diversity on population growth. *Ecol. Evol.*, 11, 17810–17816.

Smith, T.P., Clegg, T., Bell, T. & Pawar, S. (2021). Systematic variation in the temperature dependence of bacterial carbon use efficiency. *Ecol. Lett.*, 24, 2123–2133.

Stefan, H.G. & Preud'homme, E.B. (1993). Stream Temperature Estimation from Air Temperature. *JAWRA J. Am. Water Resour. Assoc.*, 29, 27–45.

Stell, E., Warner, D., Jian, J., Bond-Lamberty, B. & Vargas, R. (2021). Spatial biases of information influence global estimates of soil respiration: How can we improve global predictions? *Glob. Change Biol.*, 27, 3923–3938.

Stinchcombe, J.R., Agrawal, A.F., Hohenlohe, P.A., Arnold, S.J. & Blows, M.W. (2008). Estimating Nonlinear Selection Gradients Using Quadratic Regression Coefficients: Double or Nothing? *Evolution*, 62, 2435–2440.

Stinchcombe, J.R., Simonsen, A.K. & Blows, Mark.W. (2014). Estimating uncertainty in multivariate responses to selection. *Evolution*, 68, 1188–1196.

Tarkington, J., Zhang, H., Azevedo, R.B.R. & Zufall, R.A. (2023). Sex, amitosis, and evolvability in the ciliate Tetrahymena thermophila. *Evolution*, 77, 36–48.

Tassone, S.J., Besterman, A.F., Buelo, C.D., Ha, D.T., Walter, J.A. & Pace, M.L. (2023). Increasing heatwave frequency in streams and rivers of the United States. *Limnol. Oceanogr. Lett.*, 8, 295–304.

US EPA, O. (2021). *Climate Change Indicators: Lake Temperature*. Available at: https://www.epa.gov/climate-indicators/climate-change-indicators-lake-temperature. Last accessed 13 December 2024.

Voronov, D.A. (2005). Calculating the intrinsic growth rate: comparison of definition and model. *Zh. Obshch. Biol.*, 66, 425–430.

Wieczynski, D.J., Singla, P., Doan, A., Singleton, A., Han, Z.-Y., Votzke, S., *et al.* (2021). Linking species traits and demography to explain complex temperature responses across levels of organization. *Proc. Natl. Acad. Sci.*, 118, e2104863118.

Wieczynski, D.J., Yoshimura, K.M., Denison, E.R., Geisen, S., DeBruyn, J.M., Shaw, A.J., *et al.* (2023). Viral infections likely mediate microbial controls on ecosystem responses to global warming. *FEMS Microbiol. Ecol.*, 99, fiad016.

Zufall, R.A., Dimond, K.L. & Doerder, F.P. (2013). Restricted distribution and limited gene flow in the model ciliate Tetrahymena thermophila. *Mol. Ecol.*, 22, 1081–1091.

640 **FIGURES**

641 **Figure 1**

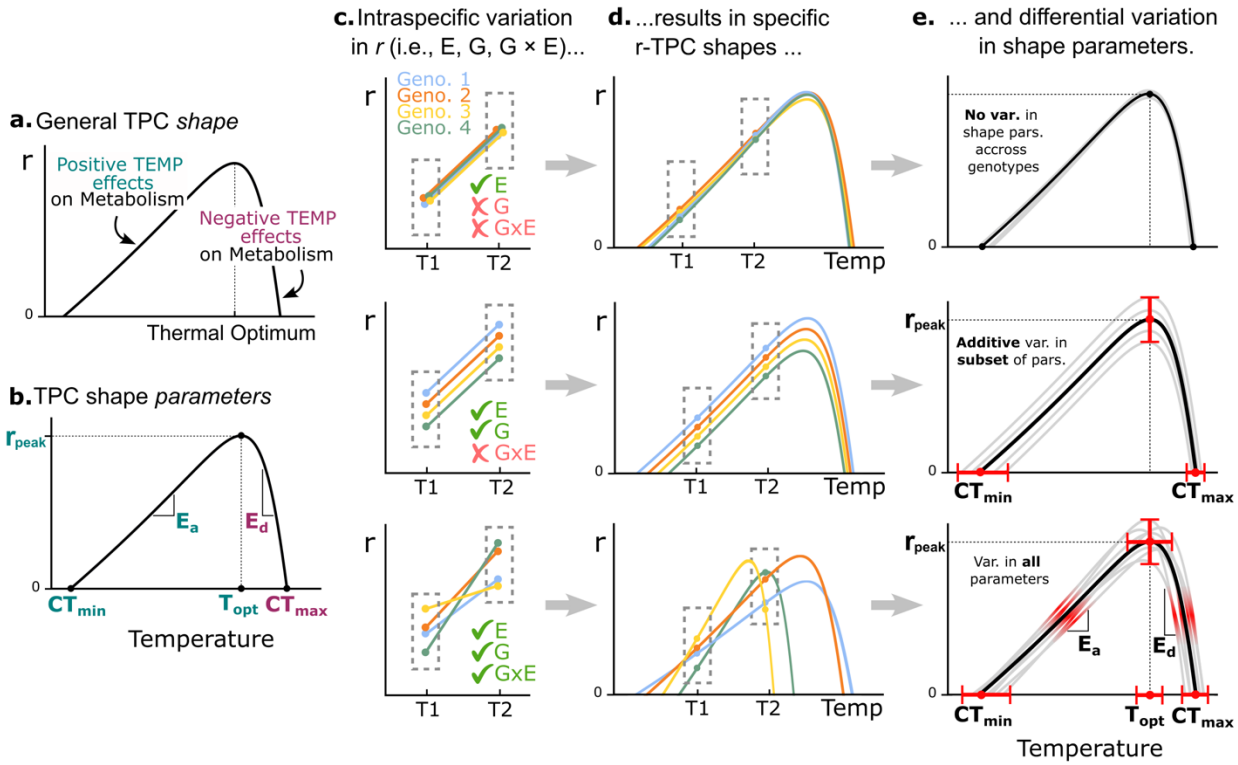

642

643

644

645

646

647

648

649

650

651

652

653

654

655

656

657

658

659

660

661

Figure 2

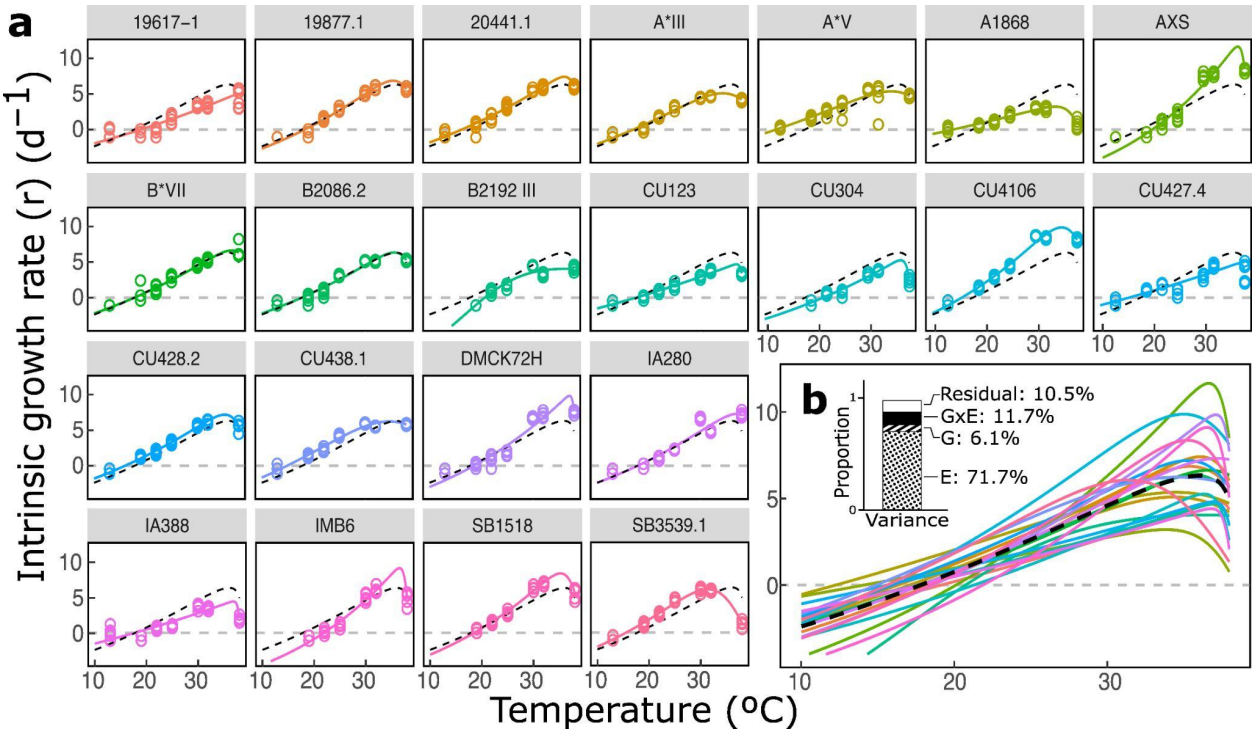
a
19617−1
19877.1
20441.1
A*III
A*V
A1868
AXS
B*VII
B2086.2
B2192 III
CU123
CU304
CU4106
CU427.4
CU428.2
CU438.1
DMCK72H
IA280
IA388
IMB6
SB1518
SB3539.1
Intrinsic growth rate (r) (d^{-1})
Temperature (ºC)
b
Residual: 10.5%
GxE: 11.7%
G: 6.1%
E: 71.7%
Proportion
Variance

Figure 3

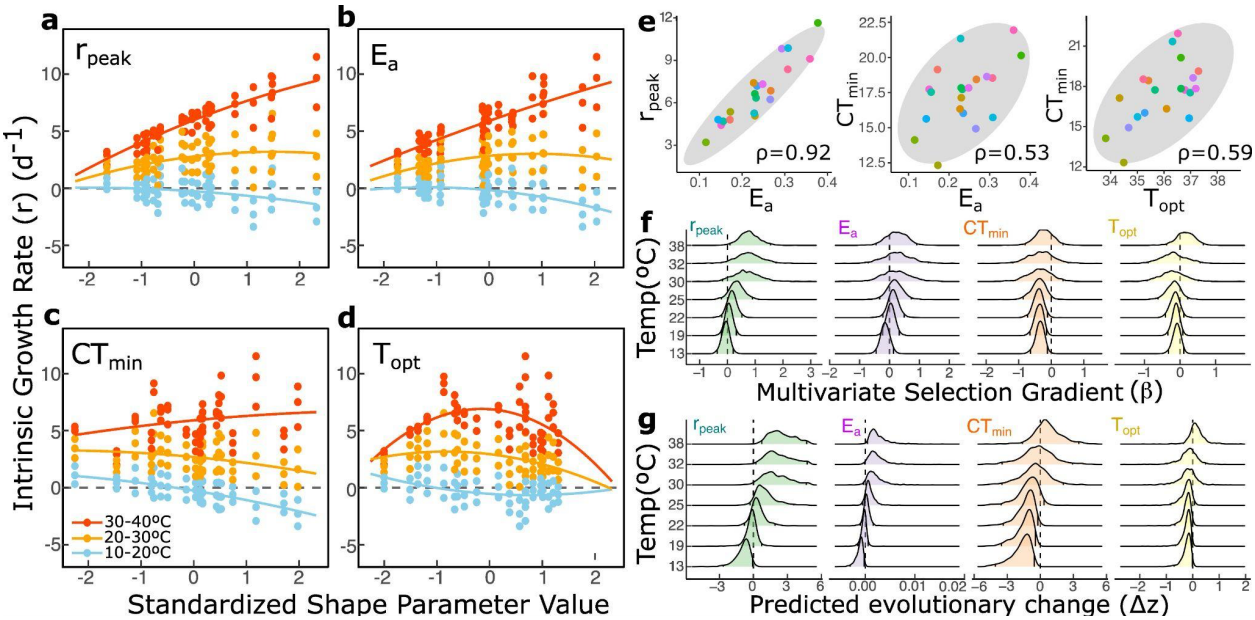
a
b
c
d
e
f
g
r_{peak}
E_a
CT_{min}
T_{opt}
Intrinsic Growth Rate (r) (d^{-1})
Standardized Shape Parameter Value
30-40ºC
20-30ºC
10-20ºC
ρ=0.92
ρ=0.53
ρ=0.59
Temp(ºC)
Multivariate Selection Gradient (β)
Predicted evolutionary change (Δz)

Figure 4

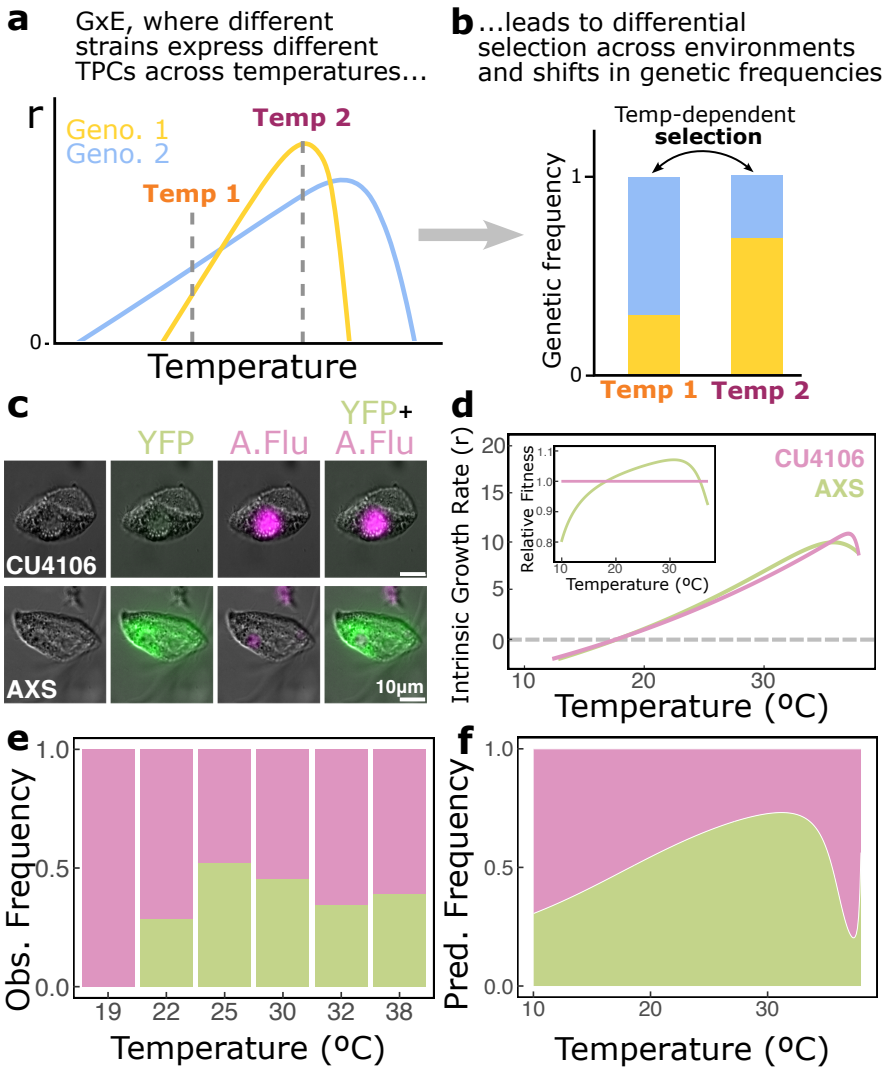
a
GxE, where different strains express different TPCs across temperatures...
r
Geno. 1
Geno. 2
Temp 2
Temp 1
0
Temperature
b
...leads to differential selection across environments and shifts in genetic frequencies
Temp-dependent selection
Genetic frequency
1
0
Temp 1
Temp 2
c
YFP
A.Flu
YFP+ A.Flu
CU4106
AXS
10µm
d
Intrinsic Growth Rate (r)
CU4106
AXS
Relative Fitness
Temperature (ºC)
e
Obs. Frequency
1.0
0.5
0.0
19
22
25
30
32
38
Temperature (ºC)
f
Pred. Frequency
1.0
0.5
0.0
10
20
30
Temperature (ºC)

729 **FIGURE LEGENDS**
730
731 **Figure 1** (a) General shape of the r-TPC. (b) r-TPC shape parameters. Blue-colored shape
732 parameters, measured in this study, include r_{peak}, E_a, CT_{min} and T_{opt}. (c) Top: environmental
733 variation (E) in *r* comes from expressing different *r* across temperatures but not genotypes, and
734 leads to overlapping reaction norms. Middle: genetic variation (G) in *r* results from expressing
735 different *r* across genotypes, but not temperatures, and leads to additive shifts in reaction norm
736 intercepts, but not slopes. Bottom: gene-by-environment interactions (G × E) results from
737 patterns expression of expression of r changing across temperature, leading to shifts in slopes of
738 reaction norms. (d) Because-rTPCs are multi-temperature reaction norms of *r*, classic
739 quantitative genetics can explain how E, G, G × E in *r* influence r-TPC shape: E in *r* produces
740 fully overlapping r-TPCs (top), G in *r* result in non-overlapping r-TPCs with genotype-specific
741 intercepts but not slopes (middle), and G × E leads to r-TPCs that vary in intercepts and slopes
742 (bottom). (e) These r-TPC shape signatures create variation in r-TPC shape parameters:
743 overlapping r-TPCs show no variation in shape parameters (top), additive shifts in r-TPC
744 intercepts lead to additive (heritable) variation in r_{peak}, CT_{min}, and CT_{max} (middle), while slope
745 and intercept variation in r-TPCs creates variation in all shape parameters.
746
747 **Figure 2** (a) Observed r-TPCs for all 22 genotypes. Dots represent observed *r* values, bold lines
748 represent Sharpe-Schoolfield model fits, and dash lines represent average TPCs across all
749 experimental genotypes. (b) All 22 TPCs are superimposed and dashed lines represent the
750 average r-TPC. Inset: amount of variation due to residual, G × E, G, and E variation in *r*.
751
752 **Figure 3** (a) Estimated adaptive landscape across temperatures (i.e., change in fitness with a
753 change in the underlying shape parameter) for r_{peak}. Color indicates temperature bins (blue: 10—
754 20ºC, yellow: 20—30ºC, red: 30—40ºC) (b) As in a, but for E_a. (c) As in a, but for CT_{min}. (d) As
755 in a, but for T_{opt}. (e) Observed genetic associations between shape parameters. Each dot is a
756 genotype color-coded as in Fig. 2. In gray, 95% confidence ellipses. ρ represents correlation
757 coefficients. (f) Estimated multivariate selection coefficient (β, 95% maximum density intervals)
758 for all shape parameters across temperatures, or eco-evo landscapes(MacColl 2011). (g)
759 Predicted evolutionary change (Δz, 95% maximum density intervals) for all shape parameters,
760 across temperatures.
761
762 **Figure 4** (a) G × E variation in r-TPCs leads to differential growth of each genotype across
763 temperatures. (b) Differential growth across temperatures leads to differential selection across
764 environments and rapid shifts in genetic frequencies across temperatures. (c) First column:
765 Differential Interference Contrast (DIC) microscopy for two genotypes of the protist
766 *Tetrahymena thermophila* (CU4106 and AXS). Second column: fluorescence microscopy image
767 overlayed on DIC. Only AXS fluoresces (green) due to the expression of Yellow Fluorescent
768 Protein (YFP). Third column: as in the second column, but for autofluorescence (A. Flu, in pink),

769 which both genotypes exhibit. Fourth column: Overlayed DIC, YFP and A.Flu images showing
770 how the different strains fluoresce once all sources of fluorescence are accounted for. (d) r-TPC
771 for genotypes CU4106 and AXS. Inset: Measures of relative fitness for both CU4106 and AXS.
772 This predicts an increase in AXS frequency relative to CU4106 at intermediate temperatures
773 relative to low or high temperatures. (e) Observed genetic frequencies across temperatures. (f)
774 Predicted genetic frequencies across temperatures.
775